

# Detecting compartmental non-Gaussian diffusion with symmetrized double-PFG MRI<sup>†</sup>

Jeffrey L. Paulsen<sup>a\*</sup>, Evren Özarslan<sup>b,c,d,e</sup>, Michal E. Komlosh<sup>c,d</sup>, Peter J. Basser<sup>c</sup> and Yi-Qiao Song<sup>a</sup>



Diffusion in tissue and porous media is known to be non-Gaussian and has been used for clinical indications of stroke and other tissue pathologies. However, when conventional NMR techniques are applied to biological tissues and other heterogeneous materials, the presence of multiple compartments (pores) with different Gaussian diffusivities will also contribute to the measurement of non-Gaussian behavior. Here we present symmetrized double PFG (sd-PFG), which can separate these two contributions to non-Gaussian signal decay as having distinct angular modulation frequencies. In contrast to prior angular d-PFG methods, sd-PFG can unambiguously extract kurtosis as an oscillation from samples with isotropic or uniformly oriented anisotropic pores, and can generally extract a combination of compartmental anisotropy and kurtosis. The method further fixes its sensitivity with respect to the time dependence of the apparent diffusion coefficient. We experimentally demonstrate the measurement of the fourth cumulant (kurtosis) of diffusion and find it consistent with theoretical predictions. By enabling the unambiguous identification of contributions of compartmental kurtosis to the signal, sd-PFG has the potential to help identify the underlying micro-structural changes corresponding to current kurtosis based diagnostics, and act as a novel source of contrast to better resolve tissue micro-structure. Copyright © 2015 John Wiley & Sons, Ltd.

Additional supporting information may be found in the online version of this article at the publisher's web site.

**Keywords:** non-Gaussian diffusion; Kurtosis; double wavevector; double diffusion encoding; microscopic anisotropy; compartment shape anisotropy; restricted diffusion; diffusion correlation

## INTRODUCTION

NMR has long been used as a non-invasive probe of material micro-structure (1), with applications in medical MRI and oil well logging (2–6) through the relationship between the apparent diffusion coefficient and pore structure (2,7). In bulk fluid, the molecular diffusion displacement  $R$  is distributed in a Gaussian fashion,  $\log [P(R)] \propto R^2$ , and thus the presence of higher order terms (e.g. fourth order term, kurtosis) is a reflection of restricted diffusion. In medical MRI, the experimental detection of the fourth moment has been used for clinical indications in diffusion kurtosis imaging (DKI) and has been linked to stroke (8) and other tissue pathologies (9,10), and its direct measurement is desirable as a clinical diagnostic tool.

A complication arises in that sample heterogeneity can also contribute to deviations from a Gaussian signal decay, even in the complete absence of non-Gaussian diffusion. For example, while diffusion in bulk fluids is Gaussian, a diffusion measurement of a water and an oil vial next to each other (without imaging) would still yield non-Gaussian behavior. This is simply due to their differing diffusion coefficients and the superposition of their signals.

In the case of imaging tissue, a single voxel can contain a variety of distinct microscopic environments of differing size and anisotropy. As with the vials of water and oil, these different environments can represent independent components. Thus, while “free water” in tissue is well characterized by Gaussian diffusion (11), variations in the tissue can lead to a distribution of observed diffusivities that would still register as a fourth order decay in DKI. If these contributions could instead be separated from the

contributions to kurtosis from restricted water, these different environments could be unambiguously identified.

Isolation of hidden “local” features of restricted diffusion is still possible. For example, oscillating the gradients such that the effective

\* Correspondence to: J. L. Paulsen, Schlumberger-Doll Research, Cambridge, MA 02139, USA.

E-mail: JPausen2@slb.com

a J. L. Paulsen, Y.-Q. Song  
Schlumberger-Doll Research, Cambridge, MA 02139 USA

b E. Özarslan  
Department of Radiology, Brigham and Women's Hospital, Harvard Medical School, Boston, MA 02215 USA

c E. Özarslan, M. E. Komlosh, P. J. Basser  
Section on Tissue Biophysics and Biomimetics, PPITS, NICHD, National Institutes of Health, Bethesda, MD 20892 USA

d E. Özarslan, M. E. Komlosh  
Center for Neuroscience and Regenerative Medicine, Uniformed Services University of the Health Sciences, Bethesda, MD 20814 USA

e E. Özarslan  
Department of Physics, Boğaziçi University, Bebek, 34342 İstanbul, Turkey

<sup>†</sup> This article has been contributed to by US Government employees and their work is in the public domain in the USA.

**Abbreviations used:** ADC, apparent diffusion coefficient; PFG, pulsed-field-gradient experiment; d-PFG, double pulsed-field-gradient experiment; sd-PFG, symmetrized double pulsed-field-gradient experiment; CK, compartmental kurtosis; CSA, compartment shape anisotropy.

encoding (“ $q$ -vector”) is spun at the magic angle will average out the influence of anisotropy, both macroscopic and compartmental (12). Alternatively, correlating the direction of diffusion over successive displacements with double pulsed field gradient techniques (d-PFG) has been shown to be effective to extract “local” features of diffusion (13–15). For instance, the signal difference between parallel ( $0^\circ$ ) and anti-parallel ( $180^\circ$ ) gradients has been used to unambiguously identify restricted diffusion (13). However, the multiple diffusive displacements measured in these angular techniques are interdependent, complicating their interpretation and design.

This work identifies mirror symmetries of diffusional motion when measured over multiple displacements, and formulates two corresponding independent measures (or modes) of stationary stochastic processes (16). These modes lack the intrinsic interdependence found between measurements of two-point displacements, greatly simplifying the design of d-PFG measurements. Thus, their utilization enables a new class of techniques, where these independent modes are experimentally controlled to engineer sequences that isolate features of diffusion.

We introduce one particular implementation for MRI, the symmetrized double pulsed-field-gradient (sd-PFG) experiment. By fixing the encoding strength for both diffusion modes while varying their physical orientations, the technique can separate Gaussian and non-Gaussian diffusion processes as modulations of the NMR signal at different “angular frequencies” in isotropic and uniformly oriented anisotropic pores. Any Gaussian moment can only contribute to zero- or two-cycle modulations, whereas kurtosis will also produce a distinct four-cycle modulation. Generally, this procedure will identify a combination of compartment shape anisotropy (CSA) and compartmental kurtosis. We will describe the theory and experimental verification of the method in a well-characterized restricted diffusion phantom and a plant specimen. We also include additional detailed proofs and simulations as part of the supplementary information (SI).

## THEORY

The conventional PFG experiment uses a pair of field gradient pulses of equal duration ( $\delta$ ) and strength (but effectively in opposite directions,  $+\mathbf{g}$  and  $-\mathbf{g}$ ) separated by a time  $\Delta$ . A spin with a displacement of  $\mathbf{R}$  will acquire a phase  $\psi = \mathbf{q} \cdot \mathbf{R}$  in the limit of small pulse widths  $\delta$ , where  $\mathbf{q} = \gamma \delta \mathbf{g}$  ( $\gamma$  is the gyromagnetic ratio) (17). The d-PFG experiment (18,13,14) adds a second and independently varied PFG pair,  $\mathbf{q}_2$ , some time  $\tau_m$  after the first PFG pair,  $\mathbf{q}_1$ . The phase encoded by the d-PFG experiment is then<sup>1</sup>  $\psi = \mathbf{q}_1 \cdot \mathbf{R}_1 + \mathbf{q}_2 \cdot \mathbf{R}_2$ , where  $\mathbf{R}_1$  and  $\mathbf{R}_2$  are the net displacements occurring during  $\mathbf{q}_1$  and  $\mathbf{q}_2$ , respectively. The NMR signal without relaxation is then

$$E(\mathbf{q}_1, \mathbf{q}_2) = \langle e^{-i\mathbf{q}_1 \cdot \mathbf{R}_1 - i\mathbf{q}_2 \cdot \mathbf{R}_2} \rangle \quad [1]$$

where  $\langle \rangle$  denotes the ensemble average. In this work, we only consider  $\tau_m = 0$  and use identical diffusion times  $\Delta$  during  $\mathbf{q}_1$  and  $\mathbf{q}_2$  (Fig. 1).

In the absence of flow, the second order cumulant expansion of  $E(\mathbf{q}_1, \mathbf{q}_2)$  depends only on the mean square of the phase,  $\frac{1}{2} \langle \psi^2 \rangle$  (20). This is a function of the mean square net displacements  $\langle \mathbf{R}_1 \mathbf{R}_1^T \rangle = \langle \mathbf{R}_2 \mathbf{R}_2^T \rangle$  and their correlations  $\langle \mathbf{R}_1 \mathbf{R}_2^T \rangle = \langle \mathbf{R}_2 \mathbf{R}_1^T \rangle$ , where the equalities follow from diffusion being a stationary process and the use of identical encoding times  $\Delta$  (21). The mean square

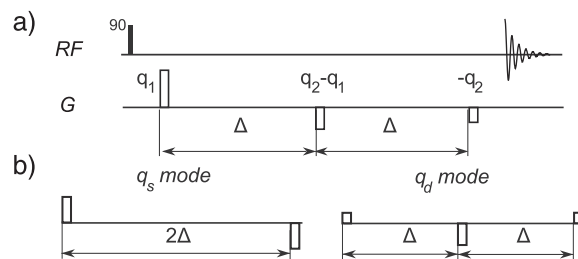


**Figure 1.** (a) The basic d-PFG pulse sequence with zero mixing time. An initial  $90^\circ$  RF pulse excites the spins, then three gradient pulses acting as two PFG encoding pairs imprint and refocus the spatial modulation of the spin magnetization across the sample, after which the signal is acquired. (b) The alternate encoding axes  $\mathbf{q}_s$  and  $\mathbf{q}_d$  are linear combinations of  $\mathbf{q}_1$  and  $\mathbf{q}_2$  that divide the total encoding period into segments of  $2\Delta$  and  $\Delta$  respectively, and are the principal signal axes.

displacement defines the diffusion tensor as a function of the diffusion time,  $\bar{\mathbf{D}}_\Delta = \langle \mathbf{R} \mathbf{R}^T \rangle / 2\Delta$ . The correlation tensor  $\langle \mathbf{R}_1 \mathbf{R}_2^T \rangle$  is also a function of the diffusion tensor, but for two different diffusion times,  $2\Delta [\bar{\mathbf{D}}_{2\Delta} - \bar{\mathbf{D}}_\Delta]$ , as shown in (19) for  $\tau_m = 0$ . With these relations, the second order moment approximation of the d-PFG signal is then

$$\ln[E(\mathbf{q}_1, \mathbf{q}_2)] \approx -\Delta [\mathbf{q}_1^T \bar{\mathbf{D}}_\Delta \mathbf{q}_1 + \mathbf{q}_2^T \bar{\mathbf{D}}_\Delta \mathbf{q}_2 + 2\mathbf{q}_1^T (\bar{\mathbf{D}}_{2\Delta} - \bar{\mathbf{D}}_\Delta) \mathbf{q}_2] \quad [2]$$

Using the basis with symmetric and anti-symmetric gradient waveforms as shown in (Fig. 1b),  $\mathbf{q}_s = (\mathbf{q}_1 + \mathbf{q}_2)$ , and  $\mathbf{q}_d = (\mathbf{q}_2 - \mathbf{q}_1)$ , Equation [2] yields

$$\ln[E(\mathbf{q}_s, \mathbf{q}_d)] \approx -\frac{\Delta}{2} [\mathbf{q}_s^T \bar{\mathbf{D}}_{2\Delta} \mathbf{q}_s + \mathbf{q}_d^T (2\bar{\mathbf{D}}_\Delta - \bar{\mathbf{D}}_{2\Delta}) \mathbf{q}_d] \quad [3]$$

Thus,  $\mathbf{q}_d$  and  $\mathbf{q}_s$  independently encode for the apparent diffusion coefficient for two different diffusion times ( $\bar{\mathbf{D}}_{2\Delta}$  and  $2\bar{\mathbf{D}}_\Delta - \bar{\mathbf{D}}_{2\Delta}$ ) and are the principal signal axes of the d-PFG experiment when  $\Delta_1 = \Delta_2$  (16). These independent encoding modes reflect a more general symmetry than Equation [3] would imply. The  $\mathbf{q}_s, \mathbf{q}_d$  decomposition also holds for all mixing times  $\tau_m$  (16), and represents the axes of mirror symmetry of the d-PFG signal as proved and simulated in the supplementary information (see SI).

By decomposing the signal equation according to these independent encoding modes, the task of designing a d-PFG experiment that isolates or intentionally correlates different terms is greatly simplified. For example, correlating the values of the apparent diffusion coefficient at different diffusion times is a matter of systematically varying the relative strengths of  $\mathbf{q}_s$  and  $\mathbf{q}_d$  (16).

Alternatively, the technique this paper introduces utilizes the  $\mathbf{q}_s, \mathbf{q}_d$  formulation to develop a sequence that removes terms in order to highlight higher order effects. Specifically, by performing the experiment holding  $|\mathbf{q}_s| = |\mathbf{q}_d| = q$  constant, it symmetrically and consistently weights the underlying encoding modes. We further focus on one specific implementation,

$$\mathbf{q}_1(\phi) = q \cos(\phi) \hat{\mathbf{x}}, \quad \mathbf{q}_2(\phi) = q \sin(\phi) \hat{\mathbf{y}} \quad [4]$$

where the angle  $\phi$  acts as a modulation phase between the magnitudes of  $\mathbf{q}_1$  and  $\mathbf{q}_2$  (Fig. 2 left). Note that the orientations of the PFG pulses do not vary. However,  $\phi$  does represent the physical orientation of the principal encoding modes relative to  $\pm \hat{\mathbf{x}}$ ,

$$\mathbf{q}_s(\phi) = q \cos(\phi) \hat{\mathbf{x}} + q \sin(\phi) \hat{\mathbf{y}}, \quad [5]$$

$$\mathbf{q}_d(\phi) = -q \cos(\phi) \hat{\mathbf{x}} + q \sin(\phi) \hat{\mathbf{y}}$$

<sup>1</sup>This notation employs a different sign convention for  $\mathbf{q}_2$  than (19), and corresponds to the first pulse of both  $\mathbf{q}_1$  and  $\mathbf{q}_2$  having positive effective gradient amplitudes.

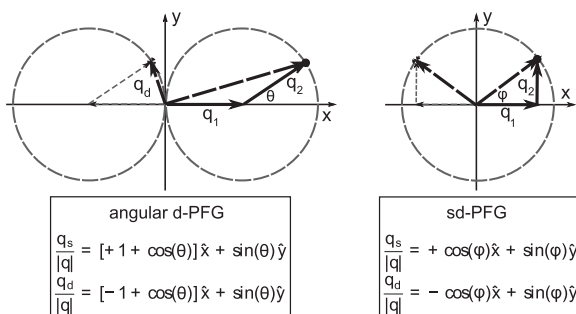


**Figure 2.** Gradient trajectories for angular d-PFG (left) and sd-PFG (right) in  $\mathbf{q}_s$ ,  $\mathbf{q}_d$  and  $\mathbf{q}_1$ ,  $\mathbf{q}_2$  coordinates. Angular d-PFG (13) fixes the magnitudes of  $\mathbf{q}_1$  and  $\mathbf{q}_2$  and varies the orientation of  $\mathbf{q}_2$ . In  $\mathbf{q}_s$ ,  $\mathbf{q}_d$  coordinates, this varies the relative magnitudes of  $\mathbf{q}_s$  and  $\mathbf{q}_d$  and so modulates the measurement's sensitivity to  $\mathbf{D}_\Delta$  and  $\mathbf{D}_{2\Delta}$ . sd-PFG modulates the relative amplitudes of  $\mathbf{q}_1$  and  $\mathbf{q}_2$ , but never orientation, in a manner so as to fix the corresponding magnitudes of  $\mathbf{q}_s$  and  $\mathbf{q}_d$  for a constant relative sensitivity to  $\mathbf{D}_\Delta$  and  $\mathbf{D}_{2\Delta}$ .

We call this specific sequence symmetrized double PFG (sd-PFG) because it symmetrically weights both the underlying encoding modes, and uniformly samples all orientations within the  $x$ - $y$ -plane for both encoding modes. As a consequence, sd-PFG modulations due to the variation in  $D_\Delta$  with  $\Delta$  for isotropic diffusion are eliminated, where Equation [3] evaluates to

$$\ln[E(q, \phi)] \approx -\Delta q^2 D_\Delta \quad [6]$$

and for anisotropic samples sd-PFG is equally sensitive to diffusion along both directions in the encoding plane, where

$$\ln[E(q, \phi)] \approx -\frac{\Delta}{2} q^2 \{ (D_{\Delta,xx} + D_{\Delta,yy}) + \cos(2\phi)(D_{\Delta,xx} - D_{\Delta,yy}) + 2 \sin(2\phi)(D_{2\Delta,xy} - D_{\Delta,xy}) \} \quad [7]$$

In contrast, traditional angular d-PFG based techniques (13) lack these symmetries (Fig. 2 left). In these experiments, the direction of motion between successive diffusion periods (instead of independent modes) is measured by fixing the magnitudes of the  $\mathbf{q}_1$  and  $\mathbf{q}_2$  encoding strengths and varying their relative orientation  $\theta$ .

$$\mathbf{q}_1(\theta) = q\hat{x}, \quad \mathbf{q}_2(\theta) = q(\cos(\theta)\hat{x} + \sin(\theta)\hat{y}) \quad [8]$$

$$\mathbf{q}_s = q((1 + \cos(\theta))\hat{x} + \sin(\theta)\hat{y}), \quad [9]$$

$$\mathbf{q}_d = q((-1 + \cos(\theta))\hat{x} + \sin(\theta)\hat{y})$$

As a result, time dependent diffusion will generally cause a  $\cos \theta$  modulation for isotropic diffusion (13,21),

$$\ln[E(q, \phi)] \approx -2\Delta q^2 \{ D_\Delta + \cos(\theta)(D_{2\Delta} - D_\Delta) \} \quad [10]$$

and will produce a stronger encoding along the direction of the first gradient pulse.

$$\ln[E(q, \phi)] \approx -\frac{1}{2}\Delta q^2 \{ 3D_{\Delta,xx} + D_{\Delta,yy} + 4 \cos(\theta)(D_{2\Delta,xx} - D_{\Delta,xx}) + 4 \sin(\theta)(D_{2\Delta,xy} - D_{\Delta,xy}) + \cos(2\theta)(D_{\Delta,xx} - D_{\Delta,yy}) + 2 \sin(2\theta)D_{\Delta,xy} \} \quad [11]$$

sd-PFG also removes the angular d-PFG modulation present when non-negligible pulse widths are employed and the  $\mathbf{q}_1$

and  $\mathbf{q}_2$  gradient pulses overlap (see SI). Then, the angular d-PFG signal oscillates even for isotropic time independent diffusion due to the encoding strength ( $b$ -value) varying (22),

$$\ln[E(g, \theta)] \approx -\frac{1}{3}g^2\delta^2(6\Delta - 2\delta - \delta \cos(\theta))D \quad [12]$$

whereas the sd-PFG signal remains constant (see SI)

$$\ln[E(g, \phi)] \approx -\frac{1}{3}g^2\delta^2(3\Delta - \delta)D \quad [13]$$

High order cumulants will cause interference-like effects, leading to additional modulations with  $\phi$  in the sd-PFG signal. The fourth cumulant, kurtosis, is the next higher moment in the cumulant expansion of the signal and will contribute to a four-cycle modulation in the sd-PFG signal as the terms  $\sin(4\phi)$  and  $\cos(4\phi)$ . Using the tensor notation in Reference (21) and assuming the narrow gradient pulse limit, the sd-PFG signal to the fourth moment is

$$\begin{aligned} \ln[E(q, \phi)] \approx & -\frac{\Delta q^2}{2}((D_{\Delta,xx} + D_{\Delta,yy}) + \cos(2\phi)(D_{\Delta,xx} - D_{\Delta,yy}) \\ & + 2\sin(2\phi)(D_{2\Delta,xy} - D_{\Delta,xy})) \\ & -\frac{q^4}{4!} \left\{ \frac{3 + \cos(4\phi)}{8}(K_{xxxx} + K_{yyyy}) \right. \\ & + \frac{\cos(2\phi)}{2}(K_{xxxx} - K_{yyyy}) + \frac{3}{4}(1 - \cos(4\phi))Z_{xyyx} \\ & \left. + \left( \sin(2\phi) - \frac{1}{2}\sin(4\phi) \right) (S_{xyyx} - S_{yyxx}) \right\} \quad [14] \end{aligned}$$

where  $\bar{K}$  reflects the mean of the fourth power of net displacement over  $\Delta$ , and the other tensors correlate  $\mathbf{R}_1$  and  $\mathbf{R}_2$  between the times defined by  $\mathbf{q}_1$  and  $\mathbf{q}_2$ . As defined in Reference (21), these are

$$\begin{aligned} K_{ijkl} &= \langle R_{1i}R_{1j}R_{1k}R_{1l} \rangle - \langle R_{1i}R_{1j} \rangle \langle R_{1k}R_{1l} \rangle \\ &\quad - \langle R_{1i}R_{1k} \rangle \langle R_{1j}R_{1l} \rangle - \langle R_{1i}R_{1l} \rangle \langle R_{1j}R_{1k} \rangle \\ Z_{ijkl} &= \langle R_{1i}R_{1j}R_{2k}R_{2l} \rangle - \langle R_{1i}R_{1j}R_{2k}R_{2l} \rangle \\ &\quad - \langle R_{1i}R_{2k} \rangle \langle R_{1j}R_{2l} \rangle - \langle R_{1i}R_{2l} \rangle \langle R_{1j}R_{2k} \rangle \\ S_{ijkl} &= \langle R_{1i}R_{1j}R_{1k}R_{2l} \rangle - \langle R_{1i}R_{1j}R_{1k}R_{2l} \rangle \\ &\quad - \langle R_{1i}R_{1k} \rangle \langle R_{1j}R_{2l} \rangle - \langle R_{1i}R_{2l} \rangle \langle R_{1j}R_{1k} \rangle \end{aligned}$$

Because kurtosis will typically induce a four-cycle modulation in the signal with respect to  $\phi$  and Gaussian terms can only cause zero- and two-cycle modulations, sd-PFG can unambiguously identify a combination of kurtosis and higher order moments of the signal decay via a Fourier decomposition of  $\ln[E(q, \phi)]$  with respect to  $\phi$ . These oscillations are a consequence of the signal equation for a tensor term of order  $2n$  involving a product of  $2n$  terms of  $\sin(\phi)$  and  $\cos(\phi)$  with sd-PFG sampling, yielding oscillations at up to  $2n$  cycles.

In comparison, correlating the direction of motion between subsequent times with angular d-PFG (13) exhibits a very different signal structure. Despite the angular d-PFG terms also consisting of trigonometric polynomials of order  $2n$ , due to the symmetry of the tensors and the  $|\mathbf{q}_1|=|\mathbf{q}_2|$  sampling, no such four-cycle oscillations are produced for kurtosis with isotropic diffusion (15,21). Thus, sd-PFG has both the advantages of removing the additional modulation due to the time dependence of the

diffusion coefficient and the ability to identify kurtosis by this Fourier analysis, including the common case of isotropic diffusion, which angular d-PFG techniques cannot do. This analysis also indicates that traditional angular d-PFG indicators of CSA can be contaminated by kurtosis. Kurtosis in angular d-PFG will still produce two-cycle modulations for isotropic pores (21), but for anisotropic pores it will also produce two- and four-cycle modulations that can be mistaken for CSA.

Typically, natural samples contain a distribution of restriction shapes and sizes, whereas the analysis so far has assumed a homogeneous sample with a single pore type. Given isotropic pores, the Fourier identification of local kurtosis is robust. In this case, the sd-PFG signal arising directly from the Gaussian moments of a heterogeneous distribution of pore sizes is simply

$$E(q, \phi) = \int dD_{\Delta} f(D_{\Delta}) e^{-\Delta q^2 D_{\Delta}} \quad [15]$$

where  $f(D_{\Delta})$  is the corresponding distribution of isotropic diffusion coefficients. A distribution  $f(D_{\Delta})$  will cause a non-Gaussian decay of  $E(q, \phi)$  as a function of  $q$ , but will maintain invariance with respect to  $\phi$ . Thus, given isotropic pores, the observation of a four-cycle modulation with sd-PFG can distinguish compartmental kurtosis (CK) from the presence of a distribution of apparent diffusion coefficients. In contrast, s-PFG measurements and current d-PFG analyses cannot make this distinction. Furthermore, these oscillating components of the sd-PFG signal can be isolated by Fourier analysis robustly, and could unambiguously identify far weaker non-Gaussian components than the traditional means of extracting kurtosis, such as fitting the second and fourth order terms from the signal  $q$ -decay.

There is an additional source to the  $4\phi$  modulation in the case of compartment shape anisotropy (CSA), where the individual pores are anisotropic but together have no net preferential orientation (see SI). Then, the two-cycle modulations in the sd-PFG signal due to local Gaussian anisotropy can combine to form a four-cycle modulation as a fourth order decay of the observed signal. A “frequency doubling” of the oscillating terms  $\cos(2\phi)$  and  $\sin(2\phi)$  occurs because the observed signal is the sum of the *exponent*, a non-linear operation, of these terms for multiple orientations. Thus, in general the observation of a four-cycle sd-PFG modulation in a heterogeneous sample reflects the presence of a combination of CSA and kurtosis as a fourth order decay.

## METHODS

We acquired sd-PFG data for a glass capillary array and a plant sample on separate instruments. To minimize artifacts, the sd-PFG sequence in figure 1a-b must be modified to include refocusing pulses, and could further utilize bipolar gradient pulses (23). For both sets of measurements, we incorporate a double spin echo during sd-PFG encoding, and use an appropriate acquisition scheme.

For the glass capillary array phantom (GCA) (PHOTONIS, Sturbridge, MA, USA), MR acquisition was carried out on a 7 T Bruker AVANCE III spectrometer with microimaging gradients (Bruker BioSpin, Billerica, MA USA) using a double-PFG filtered imaging sequence (24). The nominal pore diameter was 10  $\mu\text{m}$  with a maximum variation of 5% between capillaries. The sample temperature was set to 19 C. The sd-PFG parameters were  $\delta = 3.15$  ms,  $\Delta = 25$  ms, and  $q/2\pi = 41.9$  and 83.9  $\text{mm}^{-1}$ , respectively. The sample was placed parallel to the main magnetic field, which defines

the z-axis. The first and second gradients were fixed along the x- and y-axes, respectively. For each of the  $q$ -values, a set of 37 measurements was made with  $\phi$  values increased in increments of 10°. The imaging parameters were  $T_E = 12$  ms,  $T_R = 7$  s, slice thickness = 0.5 mm, field of view = 16  $\times$  16  $\text{mm}^2$ , matrix size = 128  $\times$  128, resolution = 0.125  $\times$  0.125  $\text{mm}^2$ , bandwidth = 50 kHz and number of averages = 2. The signal was averaged over a large region of interest of the sd-PFG images to improve the signal-to-noise ratio. To fit the observed sd-PFG signal to the simulation as in (24), a bi-compartmental model was assumed and a Levenberg–Marquardt numerical fitting procedure was employed to estimate the unknown parameters:  $S_0$  (signal with no diffusion weighting),  $f_{\text{cyl}}$  (fraction of the restricted compartment) and the inner diameter (ID). To obtain the sd-PFG signal model, we employed (SI) a general theory of NMR signal for restricted diffusion (25), which involves the generalization of the multiple correlation function method originally developed by Robertson (26) and extended by others (27,28).

For the asparagus sample, the center was cored with a 3 mm NMR tube and kept at room temperature,  $\approx 28 \pm 1$  °C. Data was collected on an Oxford 1 T horizontal bore magnet with a Bruker AVANCE II spectrometer and a custom double-PFG filtered CPMG sequence. The encoding parameters were  $\delta = 4.0$  ms,  $\Delta = 120$  ms,  $q/2\pi$  spanned 0–38.2  $\text{mm}^{-1}$  and  $\phi$  spanned 180° in 11.25° increments, omitting the angles where either  $\mathbf{q}_1$  or  $\mathbf{q}_2$  is exactly zero and fails to also act as a crusher pulse. A 16  $\times$  14 array of  $q$ -values and  $\phi$  were acquired with a CPMG acquisition employing  $TE = 0.5$  ms,  $T_R = 6$  s and eight averages. The  $q$ -values were incremented as an inner loop and the signal is normalized to the most recent  $q = 0$  acquisition to minimize the effects of temperature and other instrumental drifts.

## RESULTS AND DISCUSSION

### Glass capillary array

The distinct features of sd-PFG are the absence of modulations due to time dependence in the apparent diffusion coefficient, and a corresponding four-cycle modulation that remains even for isotropic diffusion. In contrast, when correlating the direction of motion between diffusion periods, these conditions will yield a cosine modulation due to time dependent diffusion and no modulation for isotropic kurtosis.

The GCA phantom consists of aligned cylindrical pores using capillaries (10  $\mu\text{m}$  ID) filled with water. For purely Gaussian diffusion, sd-PFG should give a constant signal as a function of  $\phi$ . However, the signal will also produce an oscillation at four cycles ( $4\phi$ ) in the presence of compartmental kurtosis. This oscillation cannot arise from CSA because the cylindrical pores are isotropic within the  $x$ – $y$ -plane. These modulations are clearly observed at high  $q$  (Fig. 3) and still observable even at lower  $q$ . This oscillation is notably absent from previous GCA measurements with angular d-PFG (24), in agreement with Jespersen’s prior predictions (21), which confirms that angular d-PFG cannot isolate CK as an oscillation for this simple pore geometry. The one-cycle oscillation characteristic of restricted diffusion in angular d-PFG ( $\cos(\theta)$ ) is notably absent from this data, in agreement with our strategy of symmetrization of the sd-PFG sampling and our  $\mathbf{q}_s, \mathbf{q}_d$  decomposition.

The observed the sd-PFG experiment signal quantitatively fits the full numerical simulation of the cylinder model. Assuming a

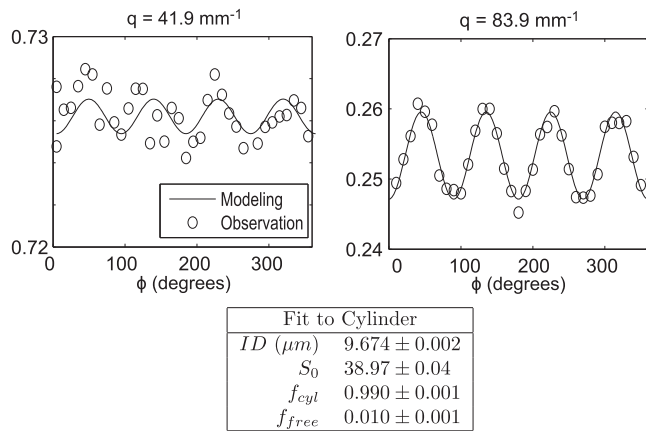


**Figure 3.** The sd-PFG signal of a glass capillary array (GCA) consisting of  $10\mu\text{m}$  ID cylinders oriented perpendicular to the gradient axes ( $g_x, g_y$ ) for low ( $41.9\text{ mm}^{-1}$ ) and higher ( $83.9\text{ mm}^{-1}$ )  $q$ . The four-cycle angular oscillation unambiguously indicates the presence of non-Gaussian diffusion. The d-PFG signal modeling is confirmed by its fit to the observed signal, where the deviations are dominated by variations in  $q$  due to gradient resolution limitations. The fitting results, assuming a cylindrical geometry and a free fluid component, yield a cylinder diameter very close to the nominal  $10\mu\text{m}$  ID of the sample's fibers.

cylindrical geometry and a variable fraction of free fluid, the fit to the data yields a diameter of  $9.67\ \mu\text{m}$  for the  $10\ \mu\text{m}$  cylinders. Deviations from the fit are dominated by the inability to maintain constant  $q$  as a function of  $\phi$  due to the limited digital resolution of the gradient electronics. The experimental gradient amplitude exhibits a noticeable variation ( $q/2\pi = 41.930 \pm 0.124\text{ mm}^{-1}$  and  $83.943 \pm 0.066\text{ mm}^{-1}$ ).

**Compartmental kurtosis in a plant sample**

The utility of the sd-PFG experiment is not when there is a homogeneous system and the observation of the bulk properties matches "local" diffusive behavior, but when there is a mixture of different environments obscuring local structure, as for restricted diffusion in samples of interest for biological and material applications. A visual analysis of the sd-PFG data, as used for the GCA, is not generally practical, because any anisotropic regions can contribute to large zero- and two-cycle modulations and visually obscure any small four-cycle signals. In this case, a harmonic decomposition by a Fourier transform of  $\ln[E(q, \phi)]$  with respect to  $\phi$  will be effective to separate Gaussian and non-Gaussian behaviors. Then the signals corresponding to the 0- and  $2\phi$  modulation should largely reflect the Gaussian moments, while the signal at the  $4\phi$  modulation can contain contributions from only higher order moments (kurtosis and CSA). We denote these components as  $E_0$  for zero angular signal modulation,  $E_2$  for the  $2\phi$  modulation,  $E_4$  for the  $4\phi$  modulation etc, and focus on only the components corresponding to the cosine transform,

$$\ln[E(q, \phi)] = E_0(q) + E_2(q)\cos(2\phi) + E_4(q)\cos(4\phi) + \dots \quad [16]$$

More generally, the oscillations of the sd-PFG signal can have non-trivial sine components (Equations [7] and [14]). Their contributions are not shown for clarity, as their amplitudes are comparatively negligible for the sample. Only  $E_2(q)$  has a significant sine component corresponding to time dependence in the cross-term of the apparent diffusion coefficient (see SI).

For the asparagus sample (Fig. 4), the constant and  $2\phi$  contributions dominate the signal, especially at small  $q$  (left panel), and the  $4\phi$  modulation is not immediately identifiable from the raw  $E(q, \phi)$  signal. However, in the frequency decomposition this  $4\phi$  modulation is clearly observable. As components with a  $n\phi$  modulation largely correspond to a  $n$ th or the first non-zero higher moment,  $E_4$  corresponds to kurtosis and its plot forms a linear curve with respect to  $q^4$ . Similarly,  $E_0$  and  $E_2$  correspond to Gaussian decays and form straight lines when plotted against  $q^2$ . The positive slopes of  $E_2(q)$  and  $E_4(q)$  do not contradict having a signal decay, and instead reflect the phase of the oscillation resulting from the structure of the corresponding diffusion tensors. For example, the positive slope of  $E_2(q)$  simply implies that  $D_{\Delta,xx} < D_{\Delta,yy}$ .

In a strict sense, the moments  $2n$  and higher will all contribute to a coefficient  $E_{2n}$  according to the moment analysis of the sd-PFG (Equations [7] and [14]). Thus,  $E_0$  and  $E_2$  will also have contributions from kurtosis and higher order moments, but these moments are typically much smaller and dominated by the

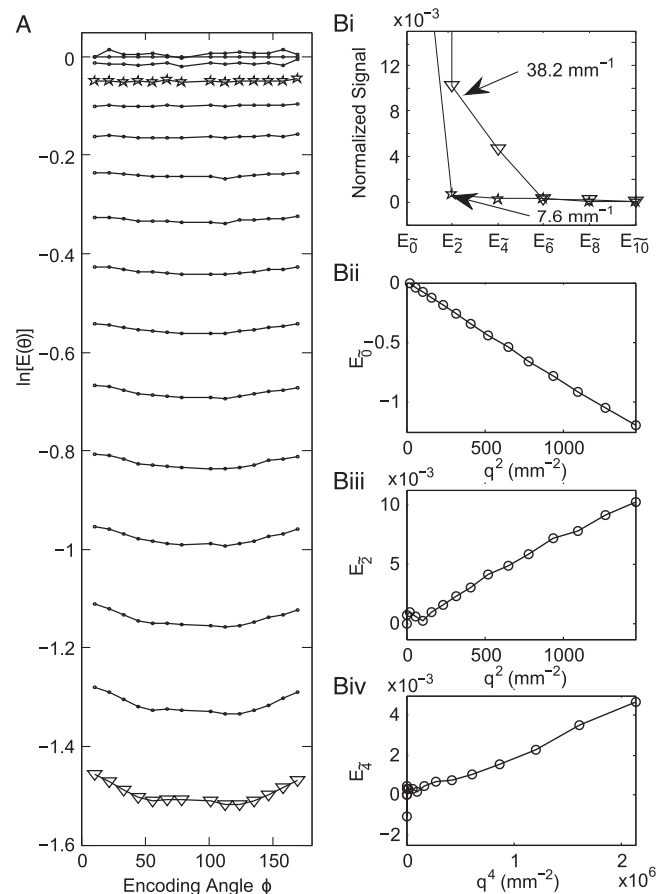


**Figure 4.** sd-PFG signal of asparagus and the Fourier analysis. (A) The raw signal as a function of  $\phi$  for different gradient pulse strengths uniformly spanning  $q=0$  to  $38.2\text{ mm}^{-1}$ . (B) The angular frequency decomposition of the signal. (i) The signal modulation as a function of angular frequency for two  $q$ -values (stars and triangles correspond to the same values of  $q$  in A). Components corresponding to a  $n\phi$  oscillation in  $\ln[E(q, \phi)]$  largely correspond to a  $n$ th moment decay (or to the first non-zero higher order moment), and so (ii)  $E_0$  and (iii)  $E_2$ , the 0 and  $2\phi$  oscillations, correspond to the Gaussian decay and form a linear curve with  $q^2$ . (iv) The plot for  $4\phi$  ( $E_4$ ) of  $\ln[E(q, \phi)]$  corresponds to kurtosis and forms a linear curve as a function of  $|q|^4$ .

lowest order term. What this relation ensures is the ability to isolate the signal from typically much larger lower order moments, and so  $E_4$  isolates the far smaller component due to kurtosis from the Gaussian contributions. This still holds true for the case of CSA, where the superposition of signal from anisotropic Gaussian diffusion can lead to a  $4\phi$  modulation, as this nonetheless only occurs for the fourth moment of the total signal (see SI). The structure of this sample allows us to rule out CSA as a contributing factor. In general, other techniques would have to be employed to differentiate CK and CSA, such as the magic-angle spinning  $q$ -vector technique of Eriksson *et al.* (12). Traditional angular d-PFG CSA indicators cannot be used to make this distinction, since these would also be affected by kurtosis.

### Generalization: correlation of independent diffusion modes

The use of principal diffusion encoding modes, as demonstrated in the design of sd-PFG with  $\mathbf{q}_s$  and  $\mathbf{q}_d$ , enables the systematic analysis and construction of the correlations between different measures of diffusion. In contrast to Mitra's initial work (13), where the relative direction of motion is compared between adjacent times ( $\mathbf{q}_1$  and  $\mathbf{q}_2$ ), the influence of basic features such as time dependent diffusion are immediately apparent and easily controlled in our framework. This greatly simplifies the design of d-PFG experiments to isolate terms as shown here, or to directly correlate them as done previously (16).

The use of these modes can enable the generation of a new class of diffusion techniques. In particular, sd-PFG is but one modulation technique possible when fixing the encoding strength for the separate diffusion modes. Instead, alternative modulation schemes could sample all the distinct angles between  $\mathbf{q}_s$  and  $\mathbf{q}_d$  in the plane, or use different fixed strengths for the two different modes. For example, in a manner analogous to Jespersen's recent approach to angular d-PFG measurements (29), the sd-PFG experiment could be repeated, varying the orientation of the encoding  $x$ - $y$ -plane between measurements to obtain rotationally invariant measures of the signal. Finally, the distinct diffusion encoding modes  $\mathbf{q}_s, \mathbf{q}_d$  are unlikely to be the only unique pair, and there are possibly many more independent modes. For example, a whole range of gradient sequences that are independent to the second moment have been incidentally identified to eliminate background gradient cross-terms (17). Whether signal from these other sequences exhibits the same mirror symmetry in the signal as  $\mathbf{q}_s, \mathbf{q}_d$  is the focus of current work.

## CONCLUSIONS

This paper describes a novel d-PFG design (sd-PFG) to directly measure compartmental non-Gaussian diffusion (e.g. kurtosis) through a unique four-cycle modulation. The presence of a diffusion distribution and bulk anisotropy in natural materials does not affect this measurement, as they appear as zero- or two-cycle modulations, easily distinguishable from the four-cycle modulation through Fourier analysis. The pulse sequence described here can be readily implemented in conventional NMR systems and on clinical MRI scanners, and the sequence parameters such as gradient strength  $q$  (up to  $40 \text{ mm}^{-1}$ ) and encoding times  $\Delta$  (10–100 ms) are well within the range of the capability of these systems. Thus, we expect this technique to find applications in medical research and clinical diagnostics to examine tissue

pathology resulting from changes in tissue microstructure. More broadly, this work identifies basic symmetries underlying multiple point diffusion measurements, and sd-PFG represents one of a new class of multi-dimensional NMR techniques based on correlating the distinct modes of diffusive motion.

## Acknowledgements

Support for this work includes contributions from Schlumberger. Evren Özarslan was supported by (i) the Department of Defense in the Center for Neuroscience and Regenerative Medicine (CNRM) and the Henry M. Jackson Foundation (HJF), (ii) NIH R01MH074794, and (iii) TÜBITAK-EU Co-Funded Brain Circulation Scheme, project 114C015. Michal Komlosch was supported by a grant for "Clinical Double Pulsed Field Gradient (dPFG) MRI for Mild TBI Assessment" under the auspices of the CNRM/HJF (# G189BH). Peter Basser was supported by funds derived from the Intramural Research Program (IRP) of the Eunice Kennedy Shriver National Institute of Child Health and Human Development (NICHD) under HD000266 (2015) "Imaging Water Diffusion in the Brain and in Other Soft Tissues".

## REFERENCES

1. Woessner DE. NMR spin-echo self-diffusion measurements on fluids undergoing restricted diffusion. *J. Phys. Chem.* 1963; 67: 1365–1367.
2. Basser P, Mattiello J, LeBihan D. MR diffusion tensor spectroscopy and imaging. *Biophys.* 1994; 66(1): 259–267.
3. Straley C, Roosini D, Vinegar H, Tutunjian P, Morriss C. Core analysis by low-field NMR. *Log. Analyst* 1997; 38: 84–94.
4. Sun B, Dunn K. Core analysis with two dimensional NMR. In *2002 International Symposium of the Society of Core Analysts, Monterey, SCA, 2002*; 22–25.
5. Jensen JH, Helpert JA, Ramani A, Hanzhang L, Kaczynski K. Diffusional kurtosis imaging: The quantification of non-gaussian water diffusion by means of magnetic resonance imaging. *Magn. Reson. Med.* 2005; 53(6): 1432–1440.
6. Kleinberg R. Well logging. *Encyclopedia of Magnetic Resonance*, 2007.
7. Mitra PP, Sen PN, Schwartz LM. Short-time behavior of the diffusion coefficient as a geometrical probe of porous media. *Phys. Rev. B* 1993; 47(14): 8565–8574.
8. Jensen JH, Falangola MF, Hu C, Tabesh A, Rapalino O, Lo C, Helpert JA. Preliminary observations of increased diffusional kurtosis in human brain following recent cerebral infarction. *NMR Biomed.* 2011; 24(5): 452–457.
9. Raab P, Hattingen E, Franz K, Zanella F E, Lanfermann H. Cerebral gliomas: Diffusional kurtosis imaging analysis of microstructural differences 1. *Radiology* 2010; 254(3): 876–881.
10. Grossman EJ, Ge Y, Jensen JH, Babb JS, Miles L, Reaume J, Silver JM, Grossman RI, Inglese M. Thalamus and cognitive impairment in mild traumatic brain injury: a diffusional kurtosis imaging study. *J. Neurotraum.* 2012; 29(13): 2318–2327.
11. Pasternak O, Sochen N, Gur Y, Intrator N, Assaf Y. Free water elimination and mapping from diffusion mri. *Magn. Reson. Med.* 2009; 62(3): 717–30.
12. Eriksson S, Lasic S, Topgaard D. Isotropic diffusion weighting in PGSE NMR by magic-angle spinning of the  $q$ -vector. *J. Magn. Reson.* 2013; 226: 13–18.
13. Mitra PP. Multiple wave-vector extensions of the NMR pulsed-field-gradient spin-echo diffusion measurement. *Phys. Rev. B* 1995; 51(21): 15074–15078.
14. Cheng Y, Cory DG. Multiple scattering by NMR. *J. Am. Chem. Soc.* 1999; 121: 7935–7936.
15. Özarslan E. Compartment shape anisotropy (CSA) revealed by double pulsed field gradient MR. *J. Magn. Reson.* 2009; 199(1): 56–67.
16. Paulsen JL, Song YQ. Two-dimensional diffusion time correlation experiment using a single direction gradient. *J. Magn. Reson.* 2014; 244: 6–11.
17. Price WS. Pulsed-field gradient nuclear magnetic resonance as a tool for studying translational diffusion: Part II. *Experimental Aspects. Concept. Magn. Reson. A* 1998; 10(4): 197–237.

18. Cory DG, Garroway AN, Miller JB. Applications of spin transport as a probe of local geometry. *Polym. Prepr. (Am. Chem. Soc., Div. Polym. Chem.)* 1990; 31(1): 149–150.
19. Jespersen SN, Buhl N. The displacement correlation tensor: Microstructure, ensemble anisotropy and curving fibers. *J. Magn. Reson.* 2011; 208: 34–43.
20. Basser P. Relationships between diffusion tensor and q-space MRI. *Magn. Reson. Med.* 2002; 47: 392–397.
21. Jespersen SN. Equivalence of double and single wave vector diffusion contrast at low diffusion weighting. *NMR Biomed.* 2012; 25: 813–818.
22. Özarslan E, Basser PJ. Microscopic anisotropy revealed by NMR double pulsed field gradient experiments with arbitrary timing parameters. *J. Chem. Phys.* 2008; 128: 154511–1.
23. Shemesh N, Özarslan E, Adiri T, Basser PJ, Cohen Y. Noninvasive bipolar double-pulsed-field-gradient NMR reveals signatures for pore size and shape in polydisperse, randomly oriented, inhomogeneous porous media. *J. Chem. Phys.* 2010; 133(4): 044705.
24. Komlosh ME, Ozarslan E, Lizak MJ, Horkay F, Schram V, Shemesh N, Cohen Y, Basser PJ. Pore diameter mapping using double pulsed-field gradient MRI and its validation using a novel glass capillary array phantom. *J. Magn. Reson.* 2011; 208(1): 128–35.
25. Özarslan E, Shemesh N, Basser PJ. A general framework to quantify the effect of restricted diffusion on the NMR signal with applications to double pulsed field gradient NMR experiments. *J. Chem. Phys.* 2009; 130(10): 104702.
26. Robertson B. Spin-echo decay of spins diffusing in a bounded region. *Phys. Rev.* 1966; 151: 273–277.
27. Barzykin AV. Exact solution of the Torrey-Bloch equation for a spin echo in restricted geometries. *Phys. Rev. B* 1998; 58: 14171–14174.
28. Grebenkov DS. NMR survey of reflected Brownian motion. *Rev. Mod. Phys.* 2007; 79: 1077–1137.
29. Jespersen SN, Lundell H, Sønderby CK, Dyrby TB. Orientationally invariant metrics of apparent compartment eccentricity from double pulsed field gradient diffusion experiments. *NMR Biomed.* 2013; 26(12): 1647–1662.

## SUPPORTING INFORMATION

Additional supporting information may be found in the online version at the publisher's web site.